Open Access

Recent Progress in Materials

LIDSEN Publishing Inc.

Technical Note

Towards Femtoscan-Assisted Analysis of Liquid Crystal Self-Organization on Different Polymer and Glass Surfaces for Lab-on-a-Chip and Lab-on-a-Dish Applications, Including Optofluidic and Flexoelectric Ones

Eugene Adamovich [1], Eugenia Buryanskaya [1], Anthon Elfimov [2], Irina Maklakova [1, 2], Oleg Gradov [1], Margaret Gradova [1], Theodor Orekhov [1, *]

1. FRC CP RAS, Kosygina str. 4, Moscow, Russia; E-Mails: neurobiophys@gmail.com; elbur@center.chph.ras.ru; eugenjournal@gmail.com; irenemaklakova@center.chph.ras.ru; retromicroscopy@gmail.com; gradov@chph.ras.ru; gradova@chph.ras.ru; theorehov@gmail.com
2. IBCP RAS, Kosygina str. 4, Moscow, Russia; E-Mails: elfim@sky.center.chph.ras.ru; camacsociety@gmail.com

* **Correspondence:** Theodor Orekhov; E-Mail: theorehov@gmail.com

Academic Editor: Stanislaw J. Klosowicz

Special Issue: Polymer Dispersed Liquid Crystal Technology

Recent Progress in Materials
2023, volume 5, issue 2
doi:10.21926/rpm.2302022

Received: December 27, 2022
Accepted: May 22, 2023
Published: May 29, 2023

Abstract

In this paper, starting with an introductory review of the applications of liquid crystals and polymer-dispersed liquid crystal systems in (bio)sensors and microfluidics, the possibilities of visualizing self-organization products of liquid crystalline media or field-induced instabilities of liquid crystalline systems are considered. In particular illustrated cases, it is proposed to use FemtoScan software-containing metrological complexes to visualize instabilities in liquid crystalline systems and products of self-organization in liquid crystalline media.

Keywords

Liquid crystal self-organization; instabilities; polymer dispersed liquid crystal; polymer lab-on-a-chip; lab-on-a-dish; flexible sensors; liquid crystal optofluidics; liquid crystal microfluidics; microfluidics; optofluidics

1. Introduction

It is well known that liquid crystals (LCs) are widely used in the development of different physical sensors, including chip-based ones [1] and lab-on-a-chip analytical systems [2]. Such LC and polymer composite structures can be used for physical [3] and chemical or biochemical sensing. Examples of LC-based physical sensors include:

1. Liquid crystal temperature sensors [4-7] (based on different principles – from optical to electrical [8, 9] and phase transition-based ones [10]), including fiber-optic liquid crystalline temperature sensors [11-13]. Thermochromic liquid crystals for thermal sensing in analytical practice can usually be introduced into microfluidic chips and thermocontrollable microreactors [14-17].
2. Liquid crystal high-pressure sensors [18-21] including fiber-optical and chip-scale microelectromechanical (MEMS-based) ones.
3. Humidity array sensors prepared with reactive cholesteric liquid crystal mesogens [22].
4. Electric field and electrostatic discharge sensors based on brightness retention of liquid crystals [23-26].
5. Different optical sensors and transducers, such as routers for optical fiber sensor networks [27], liquid crystal optical phased arrays and modulators [28, 29], fiber- and film-based spectral multiplexers [30, 31], etc.
6. Liquid crystals in optical sensors of mechanical forces and motion [32, 33]. Such systems in microfluidic polymer chips can also be used with voltage-expandable liquid crystal surfaces or liquid crystal pumps [34, 35] or liquid crystal polymer microactuators, including 3D-printed artificial cilia and artificial muscles [36-39] (electrocontrollable, thermocontrollable or photo controllable ones).
7. LC-based and LC-containing image sensors and transceivers [40], including spectrally multiplexed ones and multispectral/hyperspectral ones [41] for smart regenerative medicine of the future – for the artificial retina design [42]. Many optical sensors and transducers can also be used for multi-angle holographic detection [43, 44].

Examples of chemical sensors (including position-sensitive ones [45]) based on liquid crystals and liquid crystal polymer composites are given below:

1. pH-sensors, converters and transducers [46-49].
2. Different gas sensors (based on polymer-dispersed liquid crystals in droplets and films, planar optical waveguides and optical fibers, etc.) [50-53].
3. Toxic heavy metal detectors, including mercury [54, 55].
4. Solvent vapor detectors with cholesteric liquid crystals [56] and cholesteric liquid crystal detectors of organic vapors [57]. Such devices can be spatially sensitive/2D position-sensitive [58].

As examples of biochemical sensors based on liquid crystals and liquid crystal polymer composites (including biochemical sensing devices with *in situ*-formed liquid crystal thin films [59, 60] and microdroplets [61]) one can mention:

1. DNA biosensors on solid surfaces and liquid-crystalline DNA-based biosensors [62-64].
2. Different enzyme sensor assays and microarrays [65, 66], for example, liquid-crystal protease assays [67-69].
3. Microfluidic immunoassays with liquid crystals on the polymer biosensing chips [70].
4. Liquid crystal-based aptasensors [71-73].
5. Protein determination systems based on molecularly imprinted polymer recognition combined with birefringence liquid crystal detection [74] and liquid crystal microdroplets coated with block liquid crystalline polymers by protein adsorption for sensor applications [75]. Some LC-assisted protein detection techniques (including on-chip detection) can also be implemented using surface plasmon resonance principles [76].
6. Toxicological tests, including neurotoxicity sensors with liquid crystal components (for example, sensors for detecting organophosphorous nerve agents using liquid crystals supported on chemically functionalized surfaces [77-82] or neurochemical applications of liquid crystals sensor for organoamine detection.

Polymer microfluidic devices with liquid crystal components and devices based on LC polymers can be used for optical detection [83, 84]. For example, concentric polymer-dispersed liquid crystal rings can be used for light intensity modulation [85]. The production of interferometric sensors based on the wavelength detuning by a liquid crystalline polymer waveplate can also be implemented [86]. In the simplest case, opto-sensors can be created based on the transient property of a liquid crystal lens [87]. In chronic experiments, such sensor systems can be applied in biological objects to detect physiological and biochemical parameters of living organisms *in situ*, [88, 89]. Also such LC systems with flexoelectric response can be used as the elements of smart biocompatible implants [90-94]. Phytochemical reporters also can be liquid crystalline. As classical (since 1980th) optical reporters liquid crystal phthalocyanines [95-101] and other macroheterocyclic compounds (and also photochromic dyes with the host-guest effect of the liquid crystalline polymer matrix [102]) can be used not only in elementary physical sensors, but also in complex chemo- and biosensors.

Different LC converters of physical and chemical signals into optical ones can be used for biomedical morphochemical and morphodynamical [103-106] applications, including intraoperative [107] and implantable ones. Most progressive types of LC-assisted methods of optical spatial and spatiotemporal biological investigations in the nearest future must be associated with artificial intelligence and machine learning on the datasets of images, provided by using liquid crystalline converters [108, 109]. However, it's a very non-standard problem, because (in contrast to the additive signal) spatial or spatiotemporal behavior of liquid crystals at the microscopic and submicroscopic scales is usually associated with textural reorganization under the primary detection signals in the real physical media (or (micro)environment) and phase transitions [110-114]. This potential source of artifacts before 2000th has been eliminated by measuring area-averaged values, leveling the role of single microstructures or liquid-crystal texture elements. However, this approach is inapplicable when microanalysis with positional sensitivity is required.

Unfortunately, morphological and textural inhomogeneities and features of the spatial distribution of mesophases in contact with various substrates (metal, polymer, and glass) used in

the sensor design affect the metrological qualities of the sensors. They change not only the area-averaged analytical signal, but also its spatial distribution. The boundaries of the blurring effects of metrological signals received from liquid crystal transducers are determined by soft matter physics, that is, the partial ordering of the medium. Therefore, it is necessary not only to take into account the contribution of this (changing in response to the primary sensor signal/properties of the analyzed medium) ordering to the overall result of the analysis, but also to take into account the phenomena of microstructural self-organization and physicochemical transitions in a liquid crystal system (including LC-containing sensor sandwich systems) with positional sensitivity corresponding to the level of its structural (self) organization. In this regard, in this work, we attempt to perform a morphometric operando analysis of structural changes in a sensor based on a liquid crystal matrix on glass and polymer substrates using 3D visualization. The resulting crystals/dendrites under chemical analytics and biochemical physics detection conditions can lead to artifacts in detecting analytes and biological/biochemical/cytological structures. Therefore, we also consider examples in which the resulting products of self-organization are "artifacts" from the point of view of obtaining the final analytical signal [115, 116].

2. Materials and Methods

We used propionic acid cholesteryl ester liquid crystal (REACHEM, catalog number 070140) dissolved in chloroform (reagent grade, Chimmed, Russia). This solution was poured onto the polymer substrates made of low-density polyethylene (LDPE), in particular, those adapted for working with agar media. The latter was chosen due to the fact that visualizing sensory LC-containing systems on a chip (for which the above experiments were performed in 2018) was intended for experimental biophysical and biomedical problems. The same LCs were studied on glass substrates (as prototypes of glass microfluidic chips) [117].

The measurements were performed using an inverted microscope with a modular illuminator designed by O.V. Gradov and a modified DIC/NIC microscope. A series of raw focal scans before multi-layer image processing and stacking are given in the supplement. Image analysis was performed using FemtoScan software, designed, in particular, to analyze scanning probe and superresolution microscopy data.

3. Results

First, unification of scales and selection of the optimal mesh for 3D visualization of LC textures and crystalline mesostructures on the surface of a polymer substrate were performed. The optimal mode was established between undersampling and oversampling, when the main features of the 3D texture are already visible, but it is not overloaded with details. At the same time, we did not allow false super-resolution when the sampling increases due to bootstrap or interpolation. An example of scale selection is shown in Figure 1. Figures 1-a – 1-e demonstrate undersampling, Figures 1-g – 1-h are optimal in terms of detail, while in Figures 1-i – 1-l oversampling is observed. (Self-organization on a chip using optimal Bezier meshes we considered earlier within the context of morphological evolution in the d'Arcy-Thompson model in the technical papers [118, 119]). Using this approach, we analyzed the spatial level of self-organization, from mesoscopic to nano level. These results are a kind of resolvometry for LC medium in

response to the external factors that induce self-organization (either the nature of the surface or signals from the external environment).

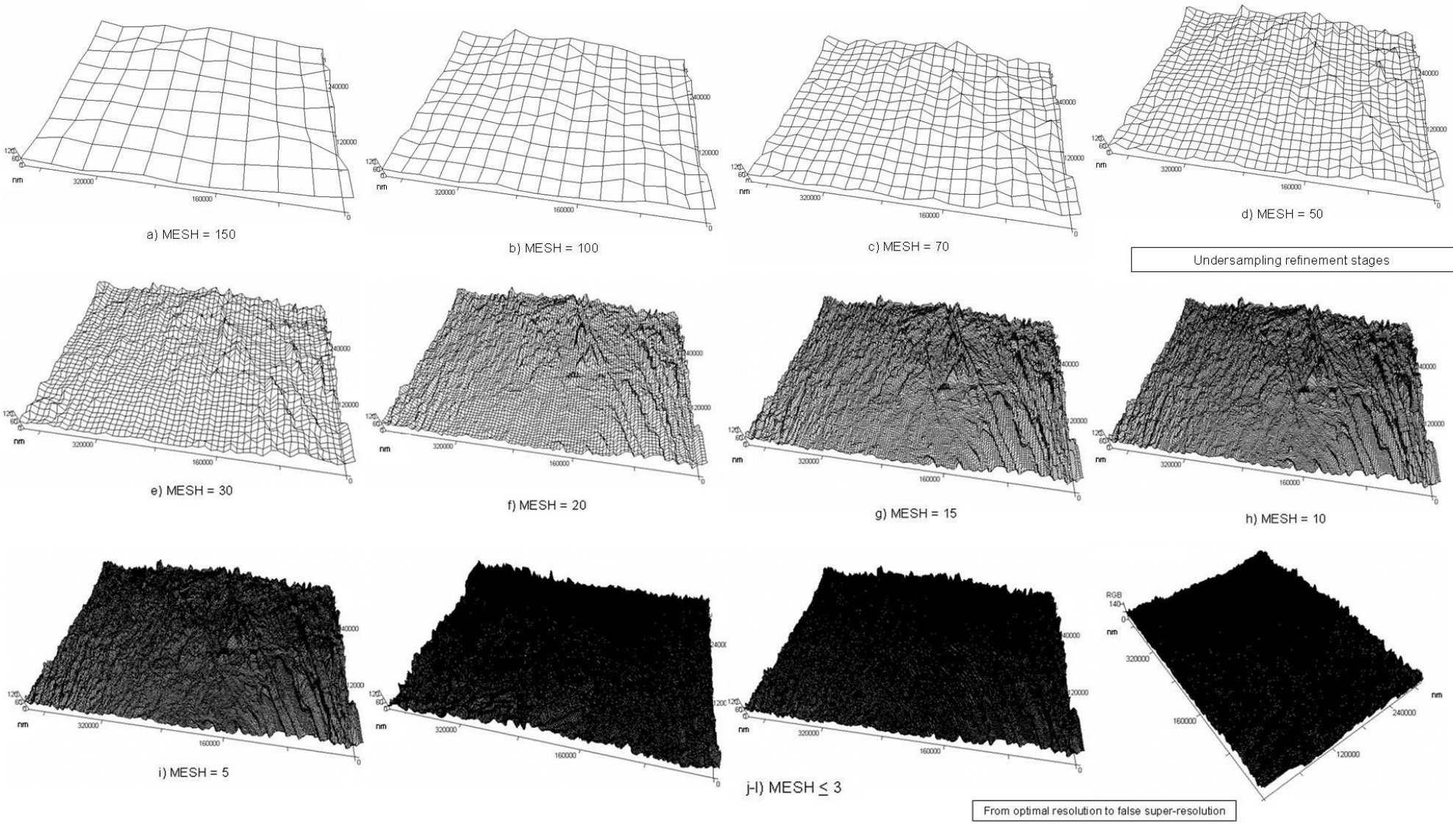

Figure 1 (a-l) Selection of the optimal LC surface visualization mode between undersampling and oversampling.

Laplace-type, Lambertian, and Lommel-Seeliger-like [120] shadow photometric mapping methods were used for pseudo-3D visualization. Pseudocolor mode enabled texture visualization, as in DIC/NIC and Hoffman and Rheinberg contrast techniques. An example of this is given in Figure 2.

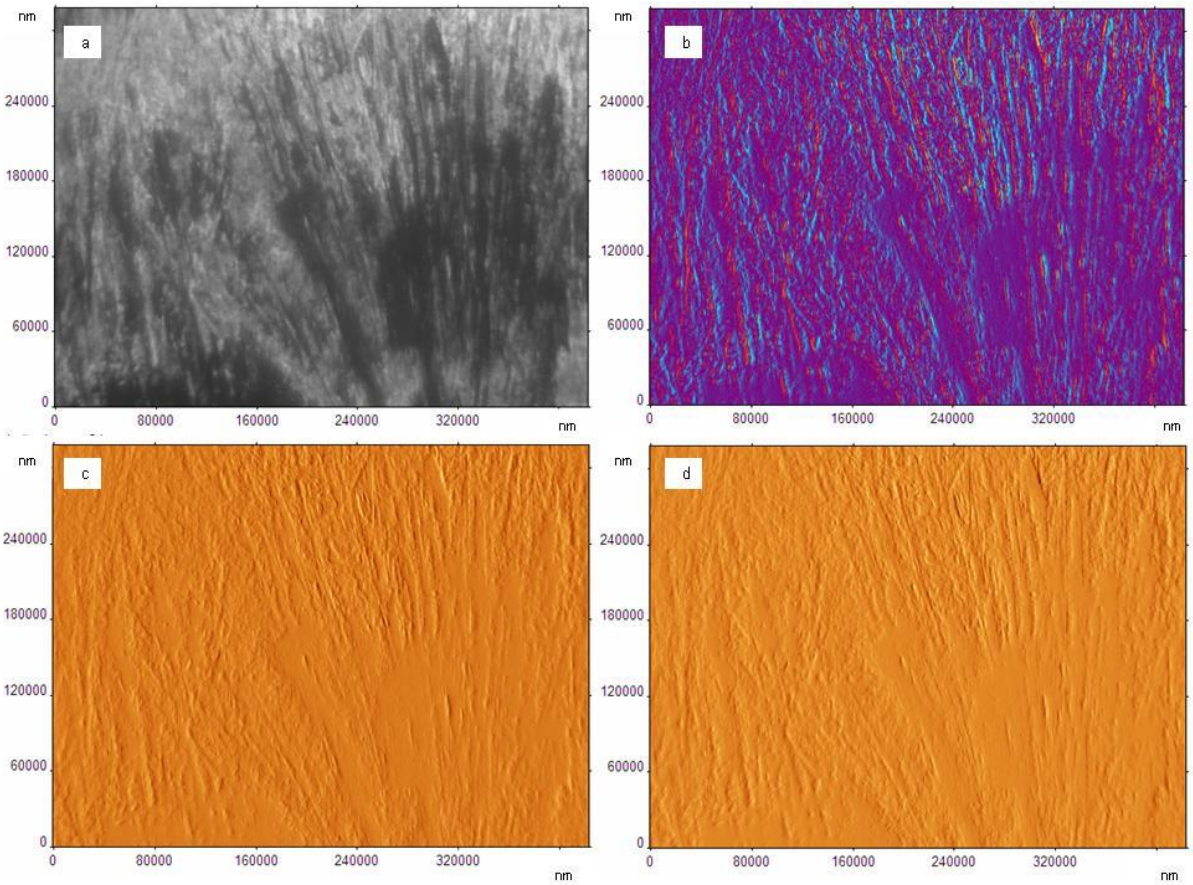

Figure 2 Laplace-type, lambertian and Lommel-Seeliger-like shadow photometric maps of the LC surface: a) grayscale monochrome image, b) visualization optimal for DIC/NIC and Rheinberg contrast; c-d) two versions of shadow-like visualizations (optimal for different shlieren techniques).

Optical density gradient fitting (including optimization in different spectrozonal channels) for 2D and 3D pseudocolor maps was also available, as shown in Figure 3. This figure and the following figures (Figure 4 – Figure 6) show the examples of linear artifacts observed in the evaporation and cooling zones.

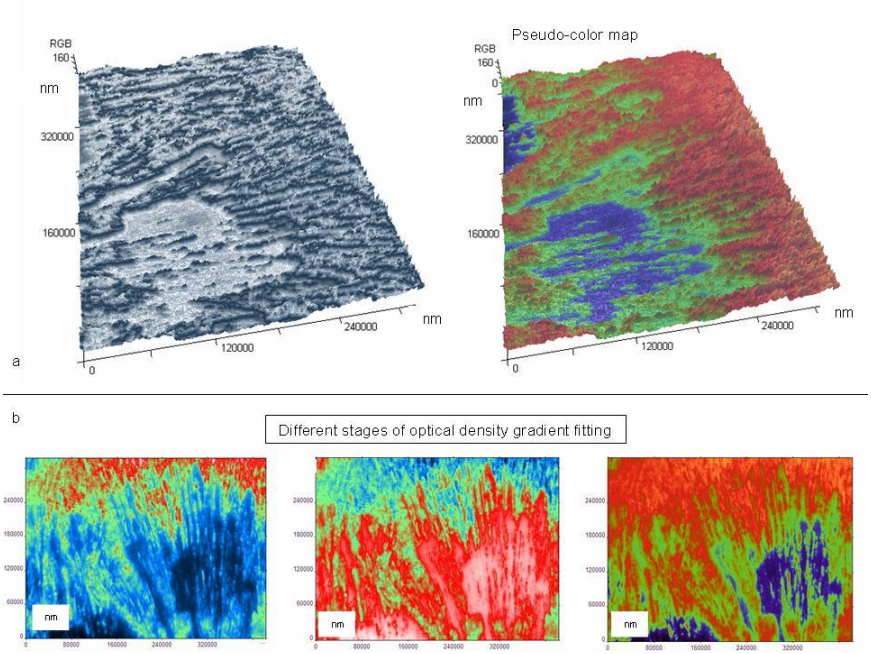

Figure 3 Optical density gradient fitting for 2D (b) and 3D pseudo-color (a) photometric maps.

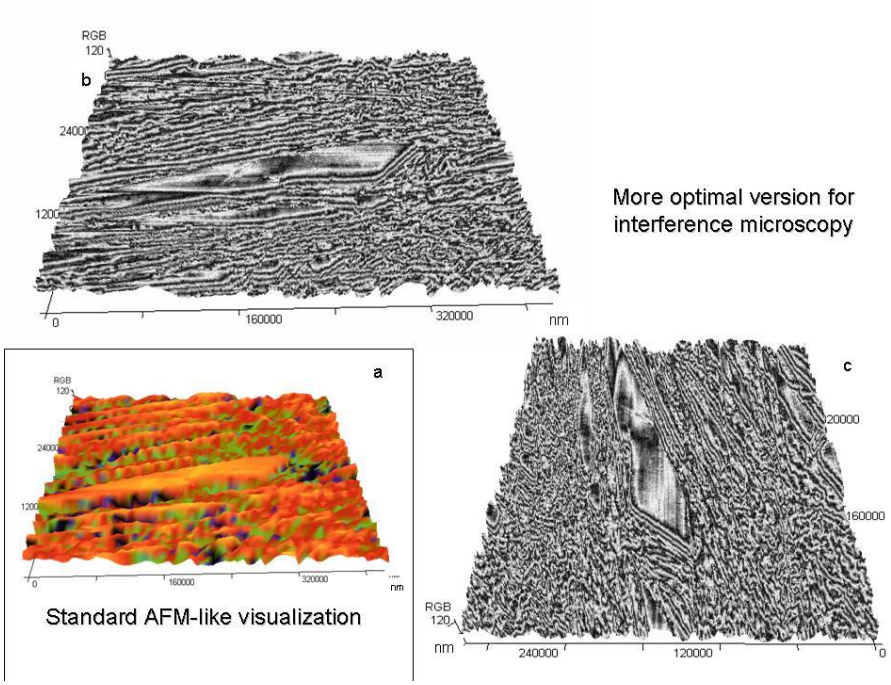

Figure 4 "Moire pattern-like" ("moire fringe-like") visualizations of examples of linear artifacts observed in the evaporation and cooling zones (optimal for MIM, VI-DIC, AFM, STM, etc.).

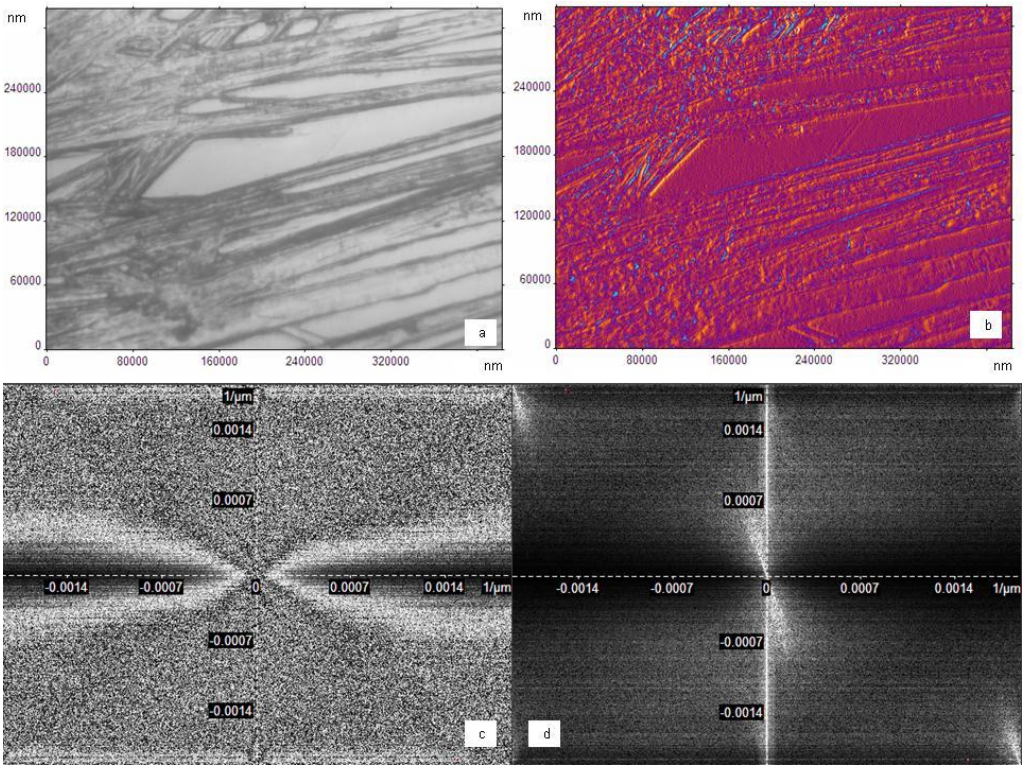

Figure 5 Correlation spectral analysis based on 2D Fourier spectra (c, d) applied for original monochrome grayscale image (a) and its volume (2D-to-3D) transform (b).

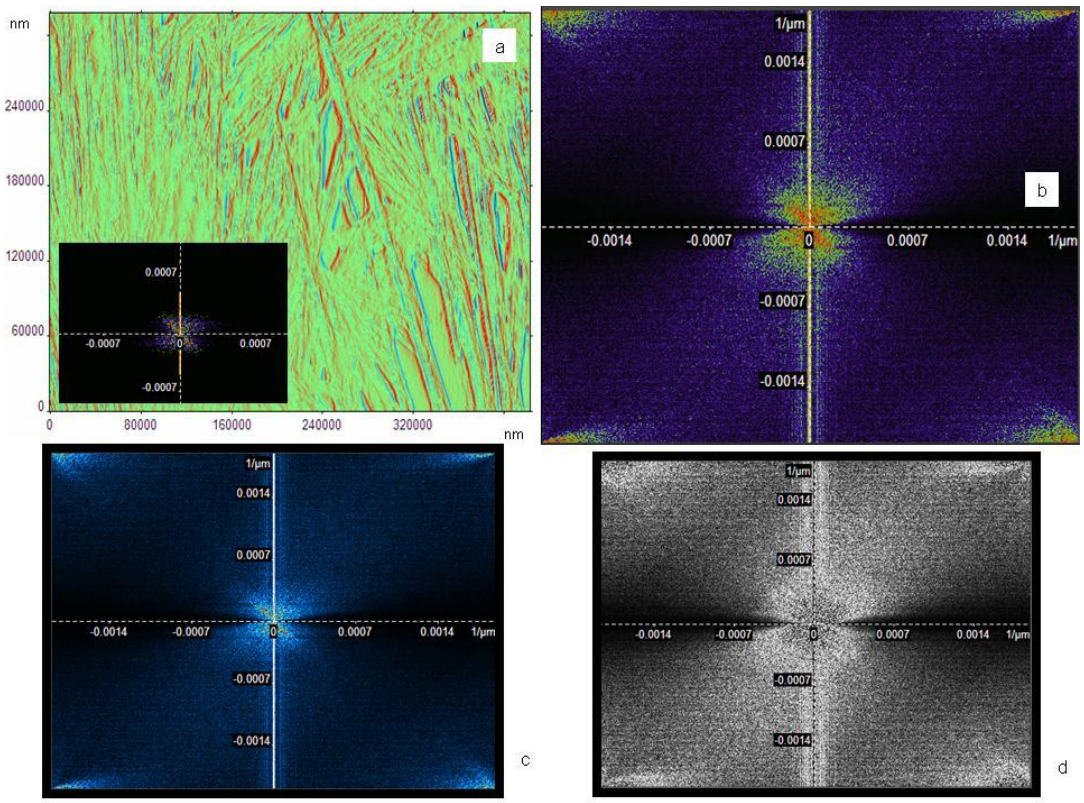

Figure 6 Examples of 2D Fourier spectra (b-d) of the original LC surface image (a).

In general, it was possible to achieve optimal visualization for probe types of microscopy (for example, AFM) and for interference methods such as modulation interference microscopy (examples of such visualizations are given in Figure 4).

Correlation spectral analysis methods based on 2D Fourier spectra (2D FFT) were applied for original monochrome grayscale images and their 2D-to-3D transforms. Previously, we implemented this using QAVIS software based on the FFTW library. However, in Femtoscan technologies, a separate module works inside the GUI program shell for these purposes. An example of its use for the original image and the same image processed according to the above-described procedure is presented in Figure 5. Figure 6 shows a variety of visualizations of 2D Fourier spectra for a similar image from another area of the same sample.

For the characterization of the image elements by 2D FFT, there are ISC and IFC (integral spatial characteristics and frequency characteristics) calculation techniques and section techniques. We previously implemented these techniques on the basis of the software developed by a group of colleagues from the Pacific Oceanological Institute of the Far Eastern Branch of the Russian Academy of Sciences. Femtoscan does not have such features, but QAVIS can work directly with video memory with images opened in any software, including any version of Femtoscan. Thus, estimation of ISC and IFC is also possible for this kind of measurement protocol. However, the Femtoscan GUI has an option for grain analysis and comparative sectioning. An example of this module application is shown in Figure 7.

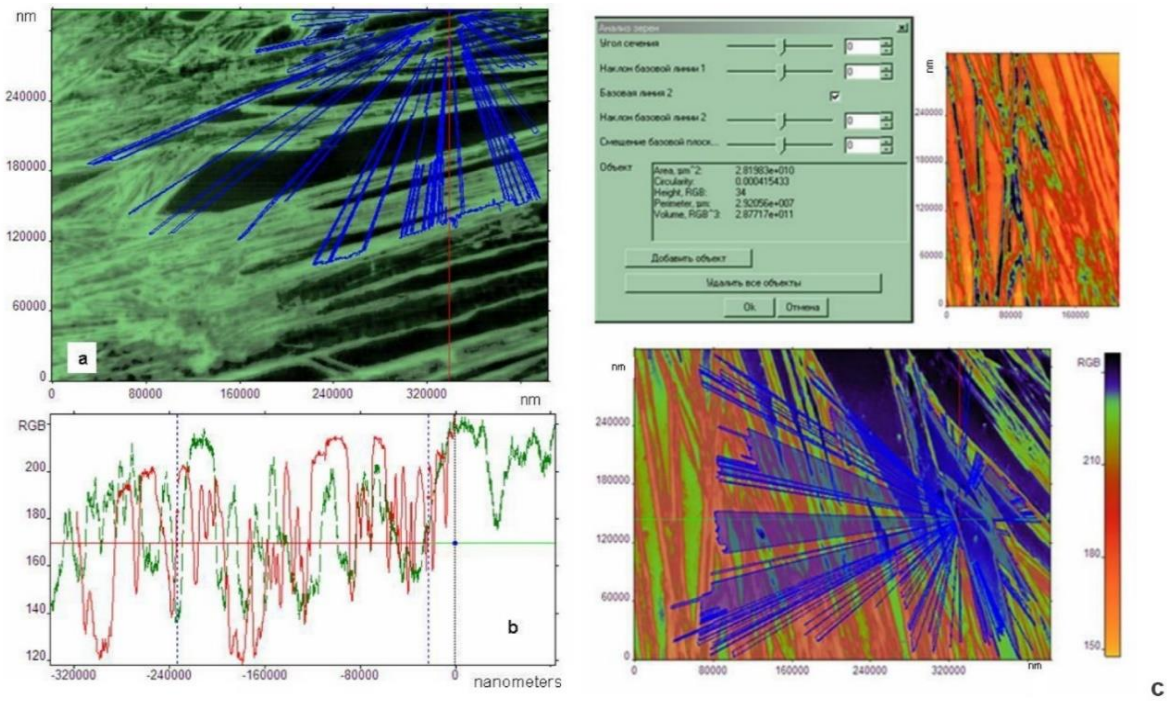

Figure 7 Section profiling and morphometric measurements of LC structures on a chip.

Macroscopic analysis of the sample surface in Petri dishes was also performed using a polariscope with the subsequent processing of video flow frames by the Sobel-Feldman gradient operator (filter).

The results are shown at the link: https://www.youtube.com/watch?v=iApqY4FRY7o (Figure 8, Figure 9). Figure 8 provided the polarization pattern image without another processing, mapping

or analysis; and Figure 9 provided the Sobel-Feldman gradient map for this pattern. In this case LC layer was used as the biochemical immobilization layer analog for the prototyping of lab-on-a-dish design. Another example of such a pattern (with its Sobel-Feldman map visualization) is provided in the video "Orientation effect detection in liquid crystals using Sobel filter (Sobel-Feldman operator). 2" by link: https://www.youtube.com/watch?v=bW7HkwkwAZw in our channel.

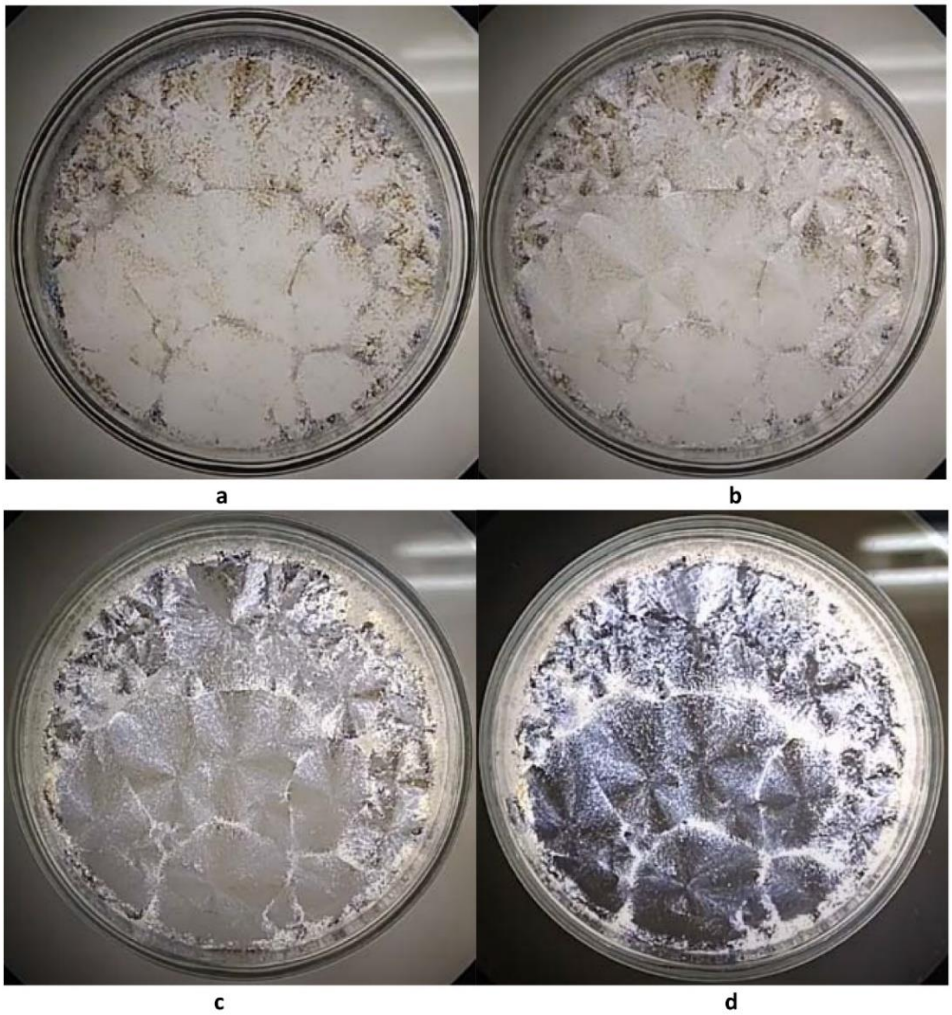

Figure 8 Polarization pattern images (registered using polariscope) of the lab-on-a-dish LC immobilization layer prototype without any digital image processing or mapping.

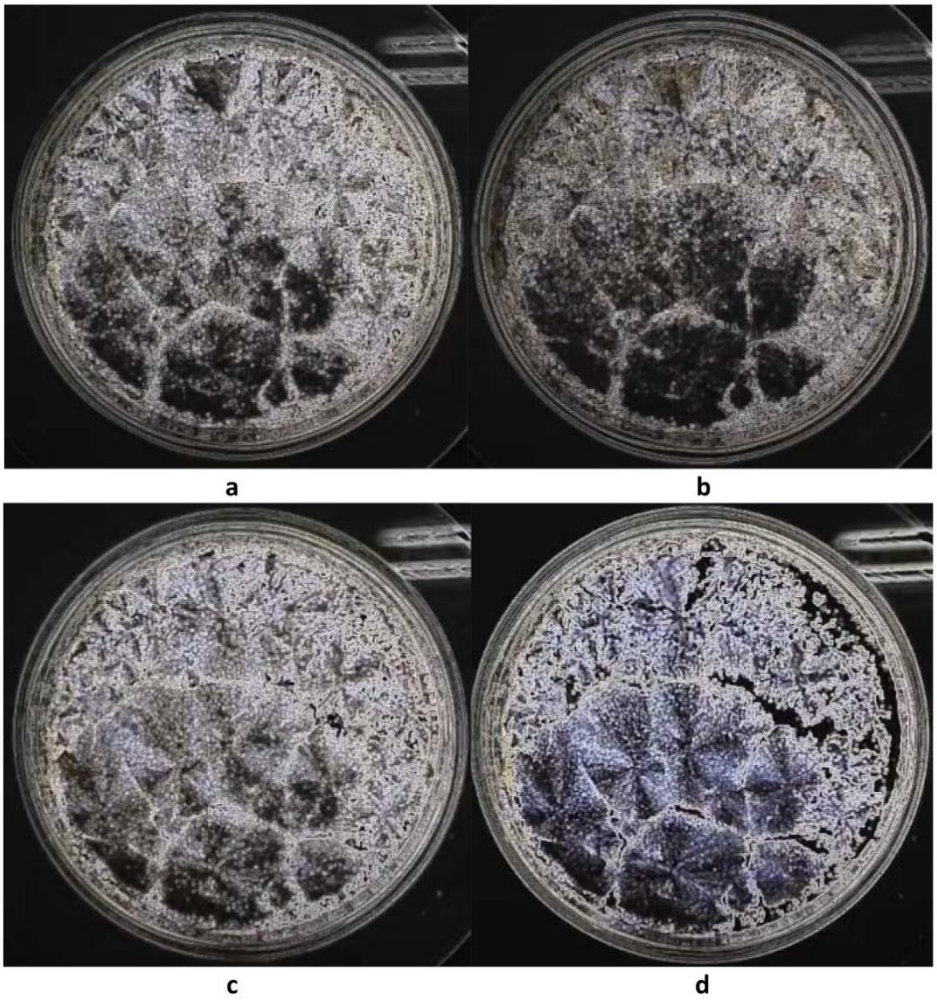

Figure 9 Sobel-Feldman [3 × 3] gradient maps of the polarization pattern images (registered using polariscope) of the lab-on-a-dish LC immobilization layer prototype.

4. Conclusions

Femtoscan allows selecting the optimal metrological mesh for analyzing self-organization and phase transitions in liquid crystals on the substrates, potentially applicable in the analytical chip design, controlling and eliminating the possible artifacts.

Femtoscan usage is compatible with Lommel-Seeliger-like techniques and edge detection techniques in multi-angle detection, which allows using together with multi-angle detection techniques on a chip containing liquid crystal structures and related elements [121, 122].

Femtoscan is compatible with the correlation-spectral analysis techniques of the structures on a chip (for example, on a chip for the analysis of liquid crystal facies [123, 124]), which allows integrating the analysis and separation (AI-clustering for their further recognition based on machine learning results) of differently organized mesophases with various textures. This can be applied to several biological and fossilization taphonomic problems [125-127].

Acknowledgments

The authors are grateful to the colleagues from M.V. Lomonosov Moscow State University for providing demo version of Femtoscan software in 2018.

Author Contributions

All authors contributed equally to this work. Conceptualization, Oleg Gradov and Theodor Orekhov; methodology, Eugene Adamovich; glasses for biomedical applications, Anthon Elfimov; AFM imaging of LCs and active polymers, Eugenia Buryanskaya; SEM imaging of LCs and active polymers, Irina Maklakova; data curation, Oleg Gradov, Eugene Adamovich; writing—original draft preparation, Eugene Adamovich, Oleg Gradov and Theodor Orekhov; writing—review and editing, Oleg Gradov, Eugene Adamovich; translation, Margaret Gradova; supervision, Theodor Orekhov; project administration, Theodor Orekhov; funding acquisition, Oleg Gradov. All authors have read and approved the publication of the manuscript.

Competing Interests

The authors have declared that no competing interests exist.

References

1. Hassanzadeh A, Lindquist RG. Liquid crystal sensor microchip. IEEE Sens J. 2011; 12: 1536-1544.
2. Khoshbin Z, Abnous K, Taghdisi SM, Verdian A. Liquid crystal-based biosensors as lab-on-chip tools: Promising for future on-site detection test kits. Trends Analyt Chem. 2021; 142: 116325.
3. Bocharov YV, Gurova IN, Kapustina OA, Remizova EI, Reshetov VN, Grigoriev SA, et al. Liquid crystal sensors of physical signals. Sens Actuator A Phys. 1991; 28: 179-183.
4. Chen CP, Jhun CG. Reflective bistable chiral splay nematic liquid crystal for low-power heat sensor. Sensors. 2020; 20: 5937.
5. Torres JC, García-Cámara B, Pérez I, Urruchi V, Sánchez-Pena JM. Wireless temperature sensor based on a nematic liquid crystal cell as variable capacitance. Sensors. 2018; 18: 3436.
6. Spinosa E, Zhong S. Application of liquid crystal thermography for the investigation of the near-wall coherent structures in a turbulent boundary layer. Sens Actuator A Phys. 2015; 233: 207-216.
7. Algorri JF, Urruchi V, Bennis N, Sánchez-Pena JM. A novel high-sensitivity, low-power, liquid crystal temperature sensor. Sensors. 2014; 14: 6571-6583.
8. Du C, Wang Q, Zhao Y. Electrically tunable long period gratings temperature sensor based on liquid crystal infiltrated photonic crystal fibers. Sens Actuator A Phys. 2018; 278: 78-84.
9. Sakata M, Hamada Y, Takeuchi K, Shibata K, Kuroki K. Characteristics of a liquid crystal IR chopper for pyroelectric IR sensors. Sens Actuator A Phys. 1994; 40: 195-201.
10. Hoshino T, Ito H, Fujieda I, Hanasaki T. Lateral solidification of a liquid crystalline semiconductor film induced by temperature gradient. Proc SPIE. 2013; 8831: 66-73.
11. Domanski AW, Wolinski TR, Borys W. Fiber-optic liquid crystalline high-sensitivity temperature sensor. Proc SPIE. 1990; 1169: 573-581.
12. Domanski AW, Kostrzewa S. Fiber optic liquid crystalline microsensor for temperature measurement in high magnetic field. Proc SPIE. 1991; 1510: 72-77.
13. He C, Korposh S, Correia R, Hayes-Gill BR, Morgan SP. Optical fibre temperature sensor based on thermochromic liquid crystal. Proc SPIE. 2019; 11199: 49-52.

14. Gillot F, Morin FO, Arata HF, Guégan R, Tanaka H, Fujita H. On-chip thermal calibration with 8 CB liquid crystal of micro-thermal device. Lab Chip. 2007; 7: 1600-1602.
15. Hoang VN, Kaigala GV, Backhouse CJ. Dynamic temperature measurement in microfluidic devices using thermochromic liquid crystals. Lab Chip. 2008; 8: 484-487.
16. Iles A, Fortt R, de Mello AJ. Thermal optimisation of the Reimer–Tiemann reaction using thermochromic liquid crystals on a microfluidic reactor. Lab Chip. 2005; 5: 540-544.
17. Segura R, Rossi M, Cierpka C, Kähler CJ. Simultaneous three-dimensional temperature and velocity field measurements using astigmatic imaging of non-encapsulated thermo-liquid crystal (TLC) particles. Lab Chip. 2015; 15: 660-663.
18. Palasagaram JN, Ramadoss R. Liquid crystal polymer based MEMS capacitive pressure sensor. Proc SPIE. 2005; 5798: 190-197.
19. Wolinski TR, Bock WJ, Konopka W, Nasilowski T, Wojcik J. Liquid crystalline optical fibers for pressure monitoring. Proc SPIE. 1996; 2836: 69-73.
20. Wolinski TR, Domanski AW, Bock WJ. All-fiber liquid crystalline hydrostatic pressure sensor. Proc SPIE. 1994; 2068: 342-347.
21. Wolinski TR, Bock WJ. Fiber optic liquid crystal high-pressure sensor. Proc SPIE. 1991; 1511: 281-288.
22. Myung DB, Hussain S, Park SY. Photonic calcium and humidity array sensor prepared with reactive cholesteric liquid crystal mesogens. Sens Actuators B Chem. 2019; 298: 126894.
23. Mathews S, Farrell G, Semenova Y. All-fiber polarimetric electric field sensing using liquid crystal infiltrated photonic crystal fibers. Sens Actuator A Phys. 2011; 167: 54-59.
24. Hotra O, Lopatynskyj I, Yavorskyj B. New electro-optical effect in nematic liquid crystal for integrated optics elements. Proc SPIE. 2003; 5124: 112-114.
25. Lin W, Sun S, Shao LY, Vai MI, Shum PP, Liu Y, et al. Tunable electro-optical and thermal optical modulator based on a liquid crystal-filled side hole fiber in fiber ring laser. IEEE Sens J. 2021; 21: 27510-27517.
26. Liang BJ, Hsu JS, Hsu PF, Liu DG. Electrostatic discharge sensor based on brightness retention of liquid crystals. IEEE Sens J. 2015; 16: 918-923.
27. Vázquez C, Pena JM, Vargas SE, Aranda AL, Pérez I. Optical router for optical fiber sensor networks based on a liquid crystal cell. IEEE Sens J. 2003; 3: 513-518.
28. Shi Y, Zhang J, Zhang Z. Experimental analysis of beam pointing system based on liquid crystal optical phase array. Photonic Sens. 2016; 6: 289-294.
29. Zeng Z, Li Z, Fang F, Zhang X. Phase compensation of the non-uniformity of the liquid crystal on silicon spatial light modulator at pixel level. Sensors. 2021; 21: 967.
30. Semenova Y, Bo L, Mathews S, Wang P, Wu Q, Farrell G. Spectral tuning of a microfiber coupler with a liquid crystal overlay. Proc SPIE. 2012; 8421: 1264-1267.
31. Sierakowski M. Liquid-crystalline filter for optical-fibre-sensors multiplexing technique. Proc SPIE. 2000; 4185: 283-286.
32. Pasechnik SV, Shmeliova DV, Tsvetkov VA, Torchinskaya AV, Chigrinov VG. Usage of liquid crystals in optical sensors of mechanical forces and motion. Proc SPIE. 2009; 7356: 396-404.
33. Chen KT, Chang CK, Kuo HL, Lee CK. Optically defined modal sensors incorporating spiropyran-doped liquid crystals with piezoelectric sensors. Sensors. 2011; 11: 1810-1818.
34. Ren H, Xu S, Wu ST. Voltage-expandable liquid crystal surface. Lab Chip. 2011; 11: 3426-3430.
35. Ren H, Xu S, Wu ST. Liquid crystal pump. Lab Chip. 2013; 13: 100-105.

36. Van Oosten CL, Bastiaansen CW, Broer DJ. Printed artificial cilia from liquid-crystal network actuators modularly driven by light. Nat Mater. 2009; 8: 677-682.
37. Lv JA, Liu Y, Wei J, Chen E, Qin L, Yu Y. Photocontrol of fluid slugs in liquid crystal polymer microactuators. Nature. 2016; 537: 179-184.
38. Shenoy DK, Thomsen III DL, Srinivasan A, Keller P, Ratna BR. Carbon coated liquid crystal elastomer film for artificial muscle applications. Sens Actuator A Phys. 2002; 96: 184-188.
39. Petsch S, Rix R, Khatri B, Schuhladen S, Müller P, Zentel R, et al. Smart artificial muscle actuators: Liquid crystal elastomers with integrated temperature feedback. Sens Actuator A Phys. 2015; 231: 44-51.
40. Efron U, Davidov I, Sinelnikov V, Levin I. CMOS-liquid-crystal-based image transceiver device. Proc SPIE. 200; 4306: 239-247.
41. Angulo LA, Parejo PG, Uribe-Patarroyo N, Alvarez-Herrero A. Hyperspectral camera based on liquid crystals for use in small satellites. Proc SPIE. 2021; 11858: 283-292.
42. Jeong J, Lee SW, Min KS, Shin S, Jun SB, Kim SJ. Liquid crystal polymer (LCP), an attractive substrate for retinal implant. Sens Mater. 2012; 24: 189-203.
43. Rutkowska KA, Kozanecka-Szmigiel A. Design of tunable holographic liquid crystalline diffraction gratings. Sensors. 2020; 20: 6789.
44. Zhang J, Carlen CR, Palmer S, Sponsler MB. Switchable holograms recorded in liquid crystalline monomers. Proc SPIE. 1994; 2042: 238-247.
45. Sutarlie L, Yang KL. Monitoring spatial distribution of ethanol in microfluidic channels by using a thin layer of cholesteric liquid crystal. Lab Chip. 2011; 11: 4093-4098.
46. Jang JH, Park SY. pH-responsive cholesteric liquid crystal double emulsion droplets prepared by microfluidics. Sens Actuators B Chem. 2017; 241: 636-643.
47. Abdolazimi V, Fontecchio AK. Liquid crystal based optical pH sensor for esophageal monitoring. Proc SPIE. 2019; 10872: 190-196.
48. Duong TD, Jang CH. Detection of arginase through the optical behaviour of liquid crystals due to the pH-dependent adsorption of stearic acid at the aqueous/liquid crystal interface. Sens Actuators B Chem. 2021; 339: 129906.
49. Kim C, Jang CH. A pH-dependent optical sensor based on ultraviolet-treated liquid crystals to detect xanthine. Sens Actuators B Chem. 2022; 372: 132652.
50. Ho WF, Chan HP, Yang KL. Planar optical waveguide platform for gas sensing using liquid crystal. IEEE Sens J. 2013; 13: 2521-2522.
51. Lai YT, Kuo JC, Yang YJ. A novel gas sensor using polymer-dispersed liquid crystal doped with carbon nanotubes. Sens Actuator A Phys. 2014; 215: 83-88.
52. Tang J, Fang J, Liang Y, Zhang B, Luo Y, Liu X, et al. All-fiber-optic VOC gas sensor based on side-polished fiber wavelength selectively coupled with cholesteric liquid crystal film. Sens Actuators B Chem. 2018; 273: 1816-1826.
53. Frazão J, Palma SI, Costa HM, Alves C, Roque AC, Silveira M. Optical gas sensing with liquid crystal droplets and convolutional neural networks. Sensors. 2021; 21: 2854.
54. Singh SK, Nandi R, Mishra K, Singh HK, Singh RK, Singh B. Liquid crystal based sensor system for the real time detection of mercuric ions in water using amphiphilic dithiocarbamate. Sens Actuators B Chem. 2016; 226: 381-387.

55. Amin NU, Siddiqi HM, Kun Lin Y, Hussain Z, Majeed N. Bovine serum albumin protein-based liquid crystal biosensors for optical detection of toxic heavy metals in water. Sensors. 2020; 20: 298.
56. Mujahid A, Stathopulos H, Lieberzeit PA, Dickert FL. Solvent vapour detection with cholesteric liquid crystals—optical and mass-sensitive evaluation of the sensor mechanism. Sensors. 2010; 10: 4887-5897.
57. Winterbottom DA, Narayanaswamy R, Raimundo Jr IM. Cholesteric liquid crystals for detection of organic vapours. Sens Actuators B Chem. 2003; 90: 52-57.
58. Liu Z, Luo D, Yang KL. Monitoring the two-dimensional concentration profile of toluene vapors by using polymer-stabilized nematic liquid crystals in microchannels. Lab Chip. 2020; 20: 1687-1693.
59. Liu Y, Cheng D, Lin IH, Abbott NL, Jiang H. Microfluidic sensing devices employing in situ-formed liquid crystal thin film for detection of biochemical interactions. Lab Chip. 2012; 12: 3746-3753.
60. Hoyle CE, Whitehead Jr JB, Brister E, Watanabe T. Kinetics of polymerization and properties of polymeric thin films generated from macroscopically oriented liquid crystalline monomers. Proc SPIE. 1994; 2042: 115-124.
61. Priest C, Quinn A, Postma A, Zelikin AN, Ralston J, Caruso F. Microfluidic polymer multilayer adsorption on liquid crystal droplets for microcapsule synthesis. Lab Chip. 2008; 8: 2182-217.
62. Munir S, Park SY. Liquid crystal-based DNA biosensor for myricetin detection. Sens Actuators B Chem. 2016; 233: 559-565.
63. Kompanets ON, Skuridin SG, Gusev VM, Kolyakov SF, Pavlov MA, Yevdokimov YM. Analytical system based on liquid-crystalline DNA particles immobilized in content of polymeric hydrogel and a portable dichrometer. Proc SPIE. 2007; 6733: 180-190.
64. Chen CH, Yang KL. Detection and quantification of DNA adsorbed on solid surfaces by using liquid crystals. Langmuir. 2010; 26: 1427-1430.
65. Duan R, Hao X, Li Y, Li H. Detection of acetylcholinesterase and its inhibitors by liquid crystal biosensor based on whispering gallery mode. Sens Actuators B Chem. 2020; 308: 127672.
66. Lu S, Guo Y, Qi L, Hu Q, Yu L. Highly sensitive and label-free detection of catalase by a H_2O_2-responsive liquid crystal sensing platform. Sens Actuators B Chem. 2021; 344: 130279.
67. Chen CH, Yang KL. Oligopeptide immobilization strategy for improving stability and sensitivity of liquid-crystal protease assays. Sens Actuators B Chem. 2014; 204: 734-740.
68. Jannat M, Yang KL. Continuous protease assays using liquid crystal as a reporter. Sens Actuators B Chem. 2018; 269: 8-14.
69. Jannat M, Yang KL. Liquid crystal-enabled protease inhibition assays developed in a millifluidic device. Sens Actuators B Chem. 2019; 296: 126595.
70. Fan YJ, Chen FL, Liou JC, Huang YW, Chen CH, Hong ZY, et al. Label-free multi-microfluidic immunoassays with liquid crystals on polydimethylsiloxane biosensing chips. Polymers. 2020; 12: 395.
71. Kim HJ, Jang CH. Liquid crystal-based aptasensor for the detection of interferon-γ and its application in the diagnosis of tuberculosis using human blood. Sens Actuators B Chem. 2019; 282: 574-579.
72. Hong PT, Jang CH. A liquid crystal sensor supported on an aptamer-immobilized surface for specific detection of ochratoxin A. IEEE Sens J. 2021; 21: 27414-27421.

73. Khoshbin Z, Verdian A, Taghdisi SM, Danesh NM, Abnous K. A novel liquid crystal assay based on aptazyme-assisted bioprobe for ultra-sensitive monitoring of lead ion. Sens Actuators B Chem. 2023; 375: 132926.
74. Cieplak M, Węgłowski R, Iskierko Z, Węgłowska D, Sharma PS, Noworyta KR, et al. Protein determination with molecularly imprinted polymer recognition combined with birefringence liquid crystal detection. Sensors. 2020; 20: 4692.
75. Khan W, Park SY. Configuration change of liquid crystal microdroplets coated with a novel polyacrylic acid block liquid crystalline polymer by protein adsorption. Lab Chip. 2012; 12:4553-4559.
76. Korec J, Stasiewicz KA, Jaroszewicz LR. SPR sensor based on a tapered optical fiber with a low refractive index liquid crystal cladding and bimetallic Ag–Au layers. Sensors. 2022; 22: 7192.
77. Cadwell KD, Lockwood NA, Nellis BA, Alf ME, Willis CR, Abbott NL. Detection of organophosphorous nerve agents using liquid crystals supported on chemically functionalized surfaces. Sen Actuators B Chem. 2007; 128: 91-98.
78. Yang KL, Cadwell K, Abbott NL. Use of self-assembled monolayers, metal ions and smectic liquid crystals to detect organophosphonates. Sens Actuators B Chem. 2005; 104: 50-56.
79. Bungabong ML, Ong PB, Yang KL. Using copper perchlorate doped liquid crystals for the detection of organophosphonate vapor. Sens Actuators B Chem. 2010; 148: 420-426.
80. VanTreeck HJ, Most DR, Grinwald BA, Kupcho KA, Sen A, Bonds MD, et al. Quantitative detection of a simulant of organophosphonate chemical warfare agents using liquid crystals. Sens Actuators B Chem. 2011; 158: 104-110.
81. Wang PH, Yu JH, Zhao YB, Li ZJ, Li GQ. A novel liquid crystal-based sensor for the real-time identification of organophosphonate vapors. Sens Actuators B Chem. 2011; 160: 929-935.
82. Chen CH, Yang KL. A liquid crystal biosensor for detecting organophosphates through the localized pH changes induced by their hydrolytic products. Sens Actuators B Chem. 2013; 181: 368-374.
83. Bayon C, Agez G, Mitov M. Wavelength-tunable light shaping with cholesteric liquid crystal microlenses. Lab Chip. 2014; 14: 2063-2071.
84. Zografopoulos DC, Asquini R, Kriezis EE, d'Alessandro A, Beccherelli R. Guided-wave liquid-crystal photonics. Lab Chip. 2012; 12: 3598-3610.
85. Hsu TC, Lu CH, Huang YT, Shih WP, Chen WS. Concentric polymer-dispersed liquid crystal rings for light intensity modulation. Sens Actuator A Phys. 2011; 169: 341-346.
86. Wierzba P. Interferometric sensor of wavelength detuning using a liquid crystalline polymer waveplate. Sensors. 2016; 16: 633.
87. Xiao H, Liu Z, Tan B, Ye M. A depth sensor based on transient property of liquid crystal lens. Photonic Sens. 2023; 13: 230230.
88. Jeong J, Lee SW, Min KS, Kim SJ. A novel multilayered planar coil based on biocompatible liquid crystal polymer for chronic implantation. Sens Actuator A Phys. 2013; 197: 38-46.
89. Hussain S, Park SY. Optical glucose biosensor based on photonic interpenetrating polymer network with solid-state cholesteric liquid crystal and cationic polyelectrolyte. Sens Actuators B Chem. 2020; 316: 128099.
90. Gradov OV, Gradova MA, Kochervinskii VV. [Biocompatible biomimetic polymer structures with an active response for implantology and regenerative medicine Part I. Basic principles of the active implant's biocompatibility]. Preprint FRC CP RAS. 2023.

91. Kochervinskii VV, Gradov OV, Gradova MA. [Ferroelectric polymers in regenerative medicine]. Genes Cells. 2019; 14: 122-123.
92. Gradov OV, Gradova MA, Kochervinskii VV. 17-Biomimetic biocompatible ferroelectric polymer materials with an active response for implantology and regenerative medicine. In: Organic ferroelectric materials and applications. Sawston: Woodhead Publishing; 2022. pp. 571-619.
93. Kochervinskii VV, Gradov OV, Gradova MA. Fluorine-containing ferroelectric polymers and their application in engineering and biomedicine. Rus Chem Rev. 2022; 91: RCR5037. doi: 10.57634/RCR5037.
94. Buryanskaya EL, Gradov OV, Gradova MA, Kiselev DA, Kochervinsky VV. [Biomedical applications of ferroelectric polymers based on vinylidene fluoride in regenerative medicine]. Genes Cells. 2022; 17: 39. doi: 10.23868/gc122163.
95. Wright JD, Roisin P, Rigby GP, Nolte RJ, Cook MJ, Thorpe SC. Crowned and liquid-crystalline phthalocyanines as gas-sensor materials. Sens Actuators B Chem. 1993; 13: 276-280.
96. Basova T, Kol'tsov E, Ray AK, Hassan AK, Gürek AG, Ahsen V. Liquid crystalline phthalocyanine spun films for organic vapour sensing. Sens Actuators B Chem. 2006; 113: 127-134.
97. Evans DR, Cook G, Saleh MA, Carns JL, Serak S, Tabiryan N. New phenomena in dye-doped liquid crystals: Black hole effect and switchable reversed diffraction. Mol Cryst Liq Cryst. 2006; 453: 177-190.
98. Kılınç N, Öztürk S, Atilla D, Gürek AG, Ahsen V, Öztürk ZZ. Electrical and NO_2 sensing properties of liquid crystalline phthalocyanine thin films. Sens Actuators B Chem. 2012; 173: 203-210.
99. Shi J, Luan L, Fang W, Zhao T, Liu W, Cui D. High-sensitive low-temperature NO_2 sensor based on Zn(II) phthalocyanine with liquid crystalline properties. Sens Actuators B Chem. 2014; 204: 218-223.
100. Gülmez AD, Polyakov MS, Volchek VV, Kostakoğlu ST, Esenpinar AA, Basova TV, et al. Tetrasubstituted copper phthalocyanines: Correlation between liquid crystalline properties, films alignment and sensing properties. Sens Actuators B Chem. 2017; 241: 364-375.
101. Sisman O, Kilinc N, Akkus UO, Sama J, Romano-Rodriguez A, Atilla D, et al. Hybrid liquid crystalline zinc phthalocyanine@Cu_2O nanowires for NO_2 sensor application. Sens Actuators B Chem. 2021; 345: 130431.
102. Ranjkesh A, Park MK, Park DH, Park JS, Choi JC, Kim SH, et al. Tilted orientation of photochromic dyes with guest-host effect of liquid crystalline polymer matrix for electrical UV sensing. Sensors. 2015; 16: 38.
103. Gradov OV, Jablokov AG. Novel morphometrics-on-a-chip: CCD- or CMOS-lab-on-a-chip based on discrete converters of different physical and chemical parameters of histological samples into the optical signals with positional sensitivity for morphometry of non-optical patterns. J Biomed Technol. 2016; 2: 1-29.
104. Gradov OV, Jablokov AG. Multiparametric lab-on-a-chip with miltiple biophysical signal converters as a novel tool for experimental stem cell biology and control equipment for hematopoetic stem cell transplantation. Cell Ther Transplant. 2017; 6: 41-42.
105. Gradov OV. Multi-functional microprobe lab-on-a-chip based on the active-pixel sensor with the position-sensitive cassette masks assembled from discrete converters of different biophysical and biochemical parameters into the optical response signals. Int J Mod Phys. 2017; 2: 23-28.

106. Gradov OV. Basic optical and corpuscular physical principles for lab-on-a-chip constructions with multiple non-optical physical signal conversions into OAS (optical analytical signals) in multiparametric experimental biomedical engineering customizations. Eur J Med Ser B. 2017; 4: 77-99.
107. Jablokov AG, Gradov OV. Multiparametric qualimetric microsurgical scanning chip-lancet model: Theoretical metrological and biomedical considerations. MicroMedicine. 2015; 3: 31-35.
108. Cao Y, Yu H, Abbott NL, Zavala VM. Machine learning algorithms for liquid crystal-based sensors. ACS Sens. 2018; 3: 2237-2245.
109. Romanov AM. Automatic classification of liquid crystal images based on topological analysis. IEEE Sens J. 2022; 23: 1377-1388.
110. Bosco A, Jongejan MG, Eelkema R, Katsonis N, Lacaze E, Ferrarini A, et al. Photoinduced reorganization of motor-doped chiral liquid crystals: Bridging molecular isomerization and texture rotation. J Am Chem Soc. 2008; 130: 14615-14624.
111. Lockwood NA, Mohr JC, Ji L, Murphy CJ, Palecek SP, De Pablo JJ, et al. Thermotropic liquid crystals as substrates for imaging the reorganization of matrigel by human embryonic stem cells. Adv Funct Mater. 2006; 16: 618-624.
112. Fonseca-Santos B, Satake CY, Calixto GM, Dos Santos AM, Chorilli M. Trans-resveratrol-loaded nonionic lamellar liquid-crystalline systems: Structural, rheological, mechanical, textural, and bioadhesive characterization and evaluation of in vivo anti-inflammatory activity. Int J Nanomedicine. 2017; 12: 6883.
113. Tamaoki N, Aoki Y, Moriyama M, Kidowaki M. Photochemical phase transition and molecular realignment of glass-forming liquid crystals containing cholesterol/azobenzene dimesogenic compounds. Chem Mater. 2003; 15: 719-726.
114. Sparavigna A, Mello A, Montrucchio B. Texture transitions in the liquid crystalline alkyloxybenzoic acid 6OBAC. Phase Transit. 2006; 79: 293-303.
115. Gradov OV. Lens-less multispectral and hyperspectral microscopy for food qualimetry. Proceedings of the Food BioTech; 2021 August 23-25; St. Petersburg, School of Biotechnology and Cryogenic Systems of ITMO University, Russia. Saint Petersburg: ITMO University Press. doi: 10.13140/RG.2.2.14082.40647.
116. Boothby JM, Kim H, Ware TH. Shape changes in chemoresponsive liquid crystal elastomers. Sens Actuators B Chem. 2017; 240: 511-518.
117. Notchenko A, Gradov O. Elementary morphometric labs-on-a-chip based on hemocytometric chambers with radiofrequency culture identification and relay of spectrozonal histochemical monitoring. Visualization Image Process Comput Biomed. 2013; 2: 2013005968. doi: 10.1615/VisualizImageProcComputatBiomed.2013005968.
118. Gradov OV. The Bezier-d'Arcy-Thompson mesh method in the reconstruction of morphogenesis and abiogenesis: An elementary biomimetic model article. Morphologia. 2011; 5: 5-23.
119. Gradoff O. Visualization of photoinduced self-organization processes in reaction-diffusion media for modelling of abiogenesis and primitive waves in morhogenesis. Int J Biophys. 2012; 2: 26-39.

120. Gradov OV, Nasirov PA, Jablokov AG. Lensless on-chip-hemocytometry with secondary processing of cell images in the framework of an unconventional photometric model. Photonics Russ. 2018; 12: 716-729.
121. Gradov OV. [Multi-angle goniometric detector for multi-parametric multi-channel analytical "lab-on-a-chip" devices based on vacuum and gas-filled chambers MAGLORS-4-VGC]. Video Science. 2018; 2: 10. doi: 10.24410/fkr7-3p42.
122. Gradov OV. Multi-Angle goniometric computer-assisted lab-on-a-chip reading system stage for vacuum-gas chambers based on analytical scanning electron microscopy platform (Goniometric CLEM Chambers). Comp Nanotechnol. 2018; 4: 9-16.
123. Tarasevich YY. Mechanisms and models of the dehydration self-organization in biological fluids. Physics Uspekhi. 2004; 47: 717-728.
124. Kistovich AV, Chashechkin YD, Shabalin VV. Formation mechanism of a circumferential roller in a drying biofluid drop. Tech Phys. 2010; 55: 473-478.
125. Gradov O. Mesophase/liquid crystal structures of wood in the regulation of carbon formation mechanisms (Dep. No. 1262/12-22; 01.11.2022; 43 p.). Min Inf Anal Bull. 2022; 12: 66.
126. Gradov OV. Evolutionary nonlinear chemistry of self-organizing mesophase/liquid crystal structures of wood from morphogenesis to regulation of carbon formation. For Bull. 2023; 27: 91-127.
127. Gradov OV. Evolution of mesophase structures in the processes of coal formation. 1st ed. Chisinau: Palmarium; 2021. 96p.